THE JOURNAL OF PHYSICAL CHEMISTRY C

Article

Cite This: J. Phys. Chem. C 2018, 122, 6340−6347

pubs.acs.org/JPCC

General Approach To Compute Phosphorescent OLED Efficiency

Xu Zhang,[†] Denis Jacquemin,[‡,§] Qian Peng,*[,∥] Zhigang Shuai,*[,†] and Daniel Escudero*[,‡]

[†]MOE Key Laboratory of Organic OptoElectronics and Molecular Engineering, Department of Chemistry, Tsinghua University, Beijing 100084, People's Republic of China

[‡]CEISAM UMR CNRS 6230, Université de Nantes, 2 rue de la Houssinière, BP 92208, 44322 Nantes Cedex 3, France

[§]Institut Universitaire de France, 1, rue Descartes, 75005 Paris Cedex 5, France

[∥]CAS Key Laboratory of Organic Solids, Institute of Chemistry of the Chinese Academy of Sciences, Beijing 100190, People's Republic of China

Supporting Information

ABSTRACT: Phosphorescent organic light-emitting diodes (PhOLEDs) are widely used in the display industry. In PhOLEDs, cyclometalated Ir(III) complexes are the most widespread triplet emitter dopants to attain red, e.g., $Ir(piq)_3$ (piq = 1-phenylisoquinoline), and green, e.g., $Ir(ppy)_3$ (ppy = 2-phenylpyridine), emissions, whereas obtaining operative deep-blue emitters is still one of the major challenges. When designing new emitters, two main characteristics besides colors should be targeted: high photostability and large photoluminescence efficiencies. To date, these are very often optimized experimentally in a trial-and-error manner. Instead, accurate predictive tools would be highly desirable. In this contribution, we present a general approach for computing the photoluminescence lifetimes and efficiencies of Ir(III) complexes by considering all possible competing excited-state deactivation processes and importantly explicitly including the strongly temperature-dependent ones. This approach is based on the combination of state-of-the-art quantum chemical calculations and excited-state decay rate formalism with kinetic modeling, which is shown to be an efficient and reliable approach for a broad palette of Ir(III) complexes, i.e., from yellow/orange to deep-blue emitters.

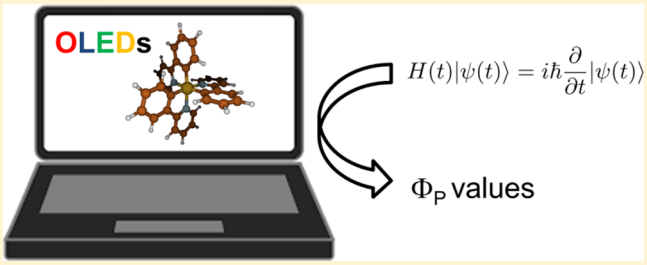

INTRODUCTION

Molecular materials modeling and virtual screening approaches are becoming fundamental tools in the design of new molecules with tailored properties,[1,2] including electroluminescent molecules.[3,4] To boost the interest of high-throughput virtual screening approaches, robust computational approaches accurately predicting all key properties are first needed. Phosphorescent organic light-emitting diodes (PhOLEDs), the so-called second generation of OLEDs,[5] are still the most widespread OLEDs technology in display industry. Therefore, enormous industrial and academic efforts are devoted to the development of new electroluminescent molecular materials with optimal performances for PhOLEDs and, in particular, to the elaboration of highly efficient and photostable deep-blue phosphors. Recent reports showed that external quantum efficiencies (EQEs) of up to 30% can be obtained using horizontally oriented heteroleptic Ir(III) complexes.[6−8] Because of the intricate nature of the competing excited-state deactivation processes in Ir(III) complexes,[9,10] the accurate computation of the photoluminescence efficiency, which is the main factor determining the EQE values in PhOLEDs, has remained elusive up to now. In practice, the efficient triplet harvesting requires an emissive triplet excited state presenting a substantial metal-to-ligand charge transfer (^{3}MLCT) character[11,12] to favor the radiative drainage to the electronic ground state over the nonradiative one. In addition, the photoluminescence lifetimes and efficiencies are temperature-dependent[10] due to the presence of thermally activated nonradiative channels associated to the population of triplet metal-centered (^{3}MC) states. The competing deactivation channels for Ir(III) complexes are illustrated in Scheme 1a, whereas the corresponding kinetic model is presented in Scheme 1b. Having in mind this kinetic model, the photoluminescence efficiencies (eq 1) and lifetimes (eq 2) can be expressed as

$$\Phi_p(T) = \frac{k_r}{k_r + k_{ISC} + k_{nr}(T)} \quad (1)$$

$$\tau(T) = \frac{1}{k_r + k_{ISC} + k_{nr}(T)} \quad (2)$$

where k_r is the ^{3}MLCT → S_0 radiative decay rate and k_{ISC} is the ^{3}MLCT → S_0 nonradiative intersystem crossing rate (ISC), which in principle is temperature-dependent through vibration population, but here it is much less pronounced because the relevant vibrational modes are of high frequency, and $k_{nr}(T)$ is the strongly temperature-dependent nonradiative decay rate associated with the population of the ^{3}MC well. The recent

Received: January 24, 2018
Revised: February 23, 2018
Published: February 27, 2018

DOI: 10.1021/acs.jpcc.8b00831
J. Phys. Chem. C 2018, 122, 6340−6347

Scheme 1. (a) Schematic Representation of the Competing Excited-State Deactivation Processes of Ir(III) Complexes;[a] (b) Kinetic Model for the Excited-State Deactivation of Ir(III) Complexes[b]

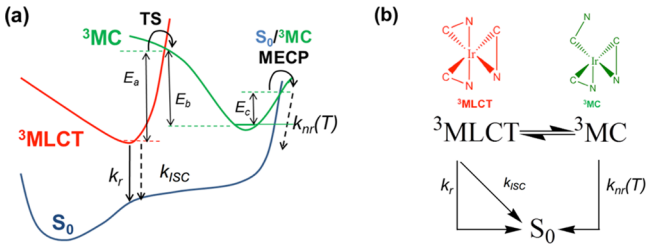

[a]Emission from the 3MLCT state (k_r) competes with the 3MLCT → S_0 nonradiative decay (k_{ISC}) and with thermally activated nonradiative decay ($k_{nr}(T)$). The latter channel is characterized by population of the ^{3}MC well through a transition state (TS) and the irreversible recovery of the ground-state (S_0) geometry through the $S_0/^3$MC minimum energy crossing point (MECP). Along this channel, the main geometrical changes occur from the 3MLCT (pseudo-octahedral) to the ^{3}MC (trigonal bipyramid) geometry through breaking of one Ir−N bond (see (b), top). Small geometrical changes occur along the ^{3}MC → MECP transformation, the latter geometry exhibiting a further distorted trigonal bipyramid arrangement. Thus, the barrier to populate the TS (E_a) is usually the rate-limiting step of this channel. For more details, see ref 18. [b]Note that singlet excited states are not included as the intersystem crossing processes present a 100% efficiency in these complexes.[11]

progresses in theoretical methods and algorithms enabled the computation of phosphorescence decay rates at the first-principles level.[13−15] Despite these progresses, the calculations of all of the nonradiative counterparts present in eq 1 have remained more cumbersome, especially the temperature-dependent decay rate, i.e., $k_{nr}(T)$. Having in mind that OLEDs should work at ambient temperatures, the accurate calculation of all decay rates is mandatory for practical applications. In fact, the two groups involved in the present work have provided preliminary kinetic models for estimating the photoluminescence efficiencies of red-to-green[16,17] and green-to-blue[18] Ir(III) complexes, respectively. A general approach valid for all kind of complexes regardless of their emission color, is still missing in the literature. Here, we fill this gap by reporting a general computational protocol to predict the photoluminescence lifetimes and efficiencies of Ir(III) complexes at any given temperature. In contrast to previous models, this protocol is in principle valid for all Ir(III) complexes, regardless of their emission color, and it is potentially transferable to other phosphor materials with similar excited-state features, e.g., square planar Pt(II) complexes. Importantly, this protocol does not rely on simplified kinetic models and does not require knowing beforehand any experimental information about the complexes, so that it can be integrated in the automated in silico prescreening of promising PhOLEDs materials.

To test the validity of this protocol, we have selected three Ir(III) complexes (see Scheme 2), i.e., *fac*-Ir(F_2ppy)(ppz)$_2$ (**1**, where ppy = 2-phenylpyridine and ppz = phenylpyrazole), *fac*-Ir(ppy)$_3$ (**2**), and *fac*-Ir(flpy)$_3$ (**3**, where flpy = 2-(9,9-dimethyl-9*H*-fluoren-2-yl)pyridine), that emit in the blue, green, and yellow/orange regions, respectively, and for which extensive experimental data is available.[10,19,20] Herein, for **1**−**3**, the k_r decay rates are determined with the Einstein relationship and the k_{ISC} decay rates are computed using the thermal vibration correlation function (TVCF) rate theory in combination with

Scheme 2. Chemical Structure of Complexes 1−3

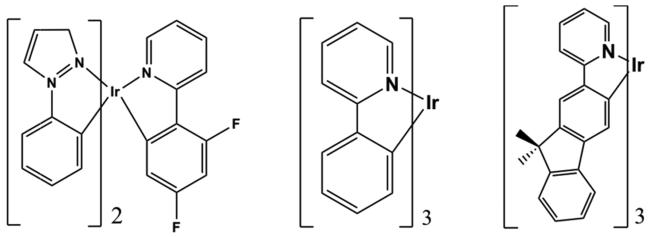

time-dependent density functional theory (TD-DFT) and DFT calculations. Regarding the calculation of k_r, it is generally accepted that perturbative approaches yield systematically slightly lower rates than nonperturbative schemes[21] or those that include spin-vibronic contributions.[17] However, these two latter sophisticated approaches are computationally more demanding and would limit the general applicability of our protocol. Moreover, it was previously found for Ir(III) complexes[22] that an optimal computational protocol based on a perturbative scheme can still provide k_r values in good agreement with the experimental ones and is therefore selected herein (see details in the Methods section). The computation of the k_{ISC} decay rates using the TVCF formalism has previously shown to yield robust results.[17,23] Finally, the $k_{nr}(T)$ decay rate is computed with canonical variational transition (CVT) state theory[24] on the basis of the computed DFT energy profiles for the thermally activated nonradiative decay (see Scheme 1a). As recently reported for these complexes,[18] the most suited kinetic model for this decay channel involves equilibration between the ^{3}MLCT and ^{3}MC states before irreversible return to the ground state. Thus,

$$^3\text{MLCT} \underset{k_b}{\overset{k_a}{\rightleftharpoons}} {}^3\text{MC} \xrightarrow{k_c} S_0 \tag{3}$$

Using the steady-state approximation and assuming this complex kinetic scenario, the $k_{nr}(T)$ decay rate has the following form

$$k_{nr}(T) = k_c k_a/(k_c + k_b) \tag{4}$$

where k_a, k_b, and k_c (i.e., k_n) can be expressed as

$$k_n = A_n \exp(-E_n/k_B T) \tag{5}$$

E_n being the activation energy; A_n, its corresponding pre-exponential factor; and k_B, the Boltzmann constant. Computing all rates in eq 4 becomes easily prohibitive for practical purposes. As detailed in ref 18, the rate-limiting step is usually the ^{3}MLCT → ^{3}MC transformation (i.e., k_a), which involves the breaking of one Ir−N bond (see Scheme 1b). Under these circumstances, eq 4 can straightforwardly be approximated as

$$k_{nr}(T) = A_0 A \exp(-E_a/k_B T) \tag{6}$$

where A_0 stands for a temperature-dependent Boltzmann prefactor in accordance to (eq 4), i.e.,

$$A_0 = \frac{1}{1 + \exp\left(\frac{E_c - E_b}{k_B T}\right)} \tag{7}$$

and A is the pre-exponential factor for the MLCT → ^{3}MC transformation, which is computed with the CVT dynamics. Equation 6 is thus capable to cover both a preequilibrated scenario as well as a non preequilibrated one. Complete details

DOI: 10.1021/acs.jpcc.8b00831
J. Phys. Chem. C 2018, 122, 6340−6347

Table 1. Experimental and Theoretical Photoluminescence Properties of 1−3

		room temperature			cryogenic temperature[c]		
	k_r (exp, s^{-1})	k_r (theo, s^{-1})	τ (exp, μs)	Φ_P (exp)	k_r (theo, s^{-1})	τ (exp, μs)	Φ_P (exp)
complex	k_{nr} (exp, s^{-1})	k_{nr} (theo, s^{-1})[d]	τ (theo, μs)	Φ_P (theo)	k_{nr} (theo, s^{-1})[d]	τ (theo, μs)	Φ_P (theo)
1[a]	4.6×10^5	3.0×10^5	1.2	0.55	1.1×10^5	3.4	[e]
	3.8×10^5	6.3×10^6	0.2	0.05	2.4×10^5	2.9	0.38
2[a]	6.1×10^5	4.1×10^5	1.6	0.97	1.9×10^5	4.0	[e]
	1.9×10^4	1.6×10^5	1.7	0.72	5.5×10^4	4.0	0.80
3[b]	2.5×10^5	2.5×10^5	1.2	0.29	2.3×10^5	4.0	[e]
	6.0×10^5	2.8×10^6	0.3	0.08	4.6×10^5	1.4	0.24

[a]Experimental values from ref 10 in 2-MeTHF. [b]Experimental values from ref 20 in toluene at RT and in toluene/ethanol/methanol (5:4:1) solutions at cryogenic temperatures. [c]Theoretical values for lifetimes computed at 150 K and for efficiencies computed at 196 K. [d]Obtained as the sum of all possible nonradiative decays. [e]Not determined experimentally.

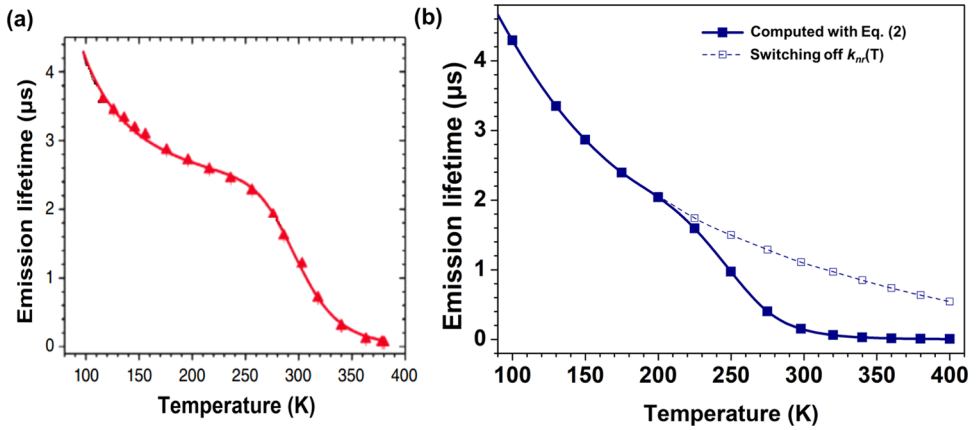

Figure 1. Experimental (a) and computed (b) temperature dependence of the photoluminescence decay using eq 2 (bold line) and switching off the $k_{nr}(T)$ component (dashed line) for **1**; (a) is adapted with permission from ref 10. Copyright 2017 American Chemical Society.

Table 2. Computed k_r, k_{ISC}, and $k_{nr}(T)$ Decay Rates, Global Lifetimes, and Φ_P Values at Different Temperatures for 1

temperature (K)	k_r (s^{-1})	k_{ISC} (s^{-1})	$k_{nr}(T)$ (s^{-1})	global lifetime (μs)	Φ_P
77	1.5994×10^4	1.7781×10^5	4.433×10^{-12}	5.1598	0.083
100	3.9948×10^4	1.9308×10^5	1.922×10^{-6}	4.2914	0.171
130	8.2342×10^4	2.1636×10^5	4.307×10^{-2}	3.3478	0.276
150	1.1326×10^5	2.3581×10^5	3.667	2.8648	0.324
175	1.5163×10^5	2.6581×10^5	2.255×10^2	2.3942	0.363
196	1.8236×10^5	2.9713×10^5	4.933×10^3	2.0405	0.384
225	2.2156×10^5	3.5286×10^5	5.366×10^4	1.5921	0.353
250	2.5211×10^5	4.1557×10^5	3.616×10^5	0.9716	0.245
275	2.7976×10^5	4.9626×10^5	1.716×10^6	0.4013	0.112
298	3.0281×10^5	6.0007×10^5	5.691×10^6	0.1516	0.046
320	3.2292×10^5	7.0711×10^5	1.522×10^7	0.0615	0.020
340	3.3971×10^5	8.3831×10^5	3.329×10^7	0.0290	0.010
360	3.5522×10^5	1.0011×10^6	6.667×10^7	0.0147	0.005
380	3.6957×10^5	1.2036×10^6	1.240×10^8	0.0080	0.003
400	3.8287×10^5	1.4561×10^6	2.166×10^8	0.0046	0.002

on the TVCF and CVT procedures can be found in the Methods section. Below we first discuss the blue emitter (**1**) in details, before presenting the results for the green (**2**) and yellow/orange (**3**) emitters.

RESULTS AND DISCUSSION

Blue-Emitter Case [*fac*-Ir(F_2ppy)(ppz)$_2$ (1)]. The temperature-dependent photoluminescence properties of complex **1** were exhaustively investigated by Thompson and co-workers.[10] Relevant experimental photoluminescence properties of **1** at cryogenic and room temperatures (RTs) are collected in Table 1. Experimentally, this blue emitter undergoes a significant drop of efficiency and lifetime at 298 K. As corroborated both experimentally[10] and theoretically,[18] this is due to the population of the thermally activated nonradiative decay process, which is readily accessible for **1** at RT as a result of its reduced E_a value. Figure 1a,b displays the recorded and computed plot of the global decay lifetime versus temperature, and the computed decay components at different temperatures are presented in Table 2. An overall qualitative and quantitative agreement of the experimental decay lifetime is recovered by the calculations. Importantly, the sigmoidlike dependence is recovered by the

DOI: 10.1021/acs.jpcc.8b00831
J. Phys. Chem. C 2018, 122, 6340−6347

computed profile. In the following, we will study in detail the origins of the drop in lifetime with increasing temperatures. In these plots, two distinct regimes are observed, a slight lifetime decrease at low temperatures and a second more significant drop at RT due to activation of the $k_{nr}(T)$ decay channel. Hence, two important inflexion points are observable, which are computed at ca. 220 and 320 K and experimentally observed at 250 and 340 K. A deeper analysis of the results (see Table 2) reveals that before the first inflexion point, in the low-temperature regime (100−200 K), only the k_r and k_{ISC} components contribute to the global lifetime (see Table 2). Because of the large ^{3}MLCT → S_0 spin−orbit couplings (SOCs), k_r is of the order of 10^5. Regarding the k_{ISC} values, they are notably influenced by the ^{3}MLCT−S_0 energy gap and by the total reorganization energies. The total reorganization energy, which is a measure of the extent of vibronic coupling between these two electronic states, is obtained as a sum over all normal mode energy times their corresponding Huang−Rhys factor. Figure 2 collects the

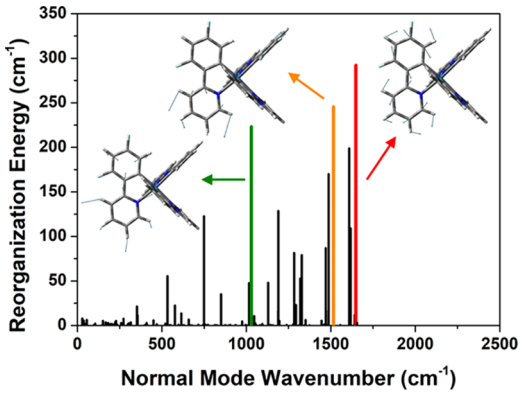

Figure 2. Calculated reorganization energies of each normal mode for **1**. The displacement vectors of its three most relevant modes are depicted.

reorganization energies of the most relevant normal modes. The normal modes in the 500−1600 cm^{-1} region predominantly contribute to the k_{ISC} value of **1** (see the displacement vectors of its three most relevant modes in Figure 2, which involve aromatic C=C stretchings and in-plane deformations of mainly the (F_2ppy) ligand). As the relevant vibrational modes are of high frequency, there is only a slight increase of k_{ISC} with temperature (see Table 1). Finally, $k_{nr}(T)$ originates from the thermally activated formation of the ^{3}MC state through the rupture of one Ir−N coordinating bond (see Scheme 1). To perform the CVT dynamics, the relevant stationary points of the rate-limiting step, i.e., ^{3}MLCT → TS → ^{3}MC, were optimized and subsequently intrinsic reaction coordinate (IRC) calculations were carried out in both forward and backward directions (B3LYP/6-31G(d,p)/LANL2DZ). In Figure 3, the corresponding IRC including selected geometries along the path is plotted. The ^{3}MLCT → TS → ^{3}MC path is characterized by two main reaction coordinates: Ir−N bond stretching (from 2.18 to 3.43 Å) and an increase in the $\phi_{1,2,3,4}$ dihedral angle (from 3 to 60°, see Figure 3). Herein, one critical aspect that needs to be mastered for the CVT simulations is the accurate estimation of E_a because, due to their exponential relationship, small deviations in the energies imply huge changes in the decay rates (see eq 6). Toward this end, on the basis of previous studies on the activation energies of 5d transition-metal complexes,[25] the double-hybrid functional including dispersion PWPB95-D3 is chosen herein. The results of the CVT simulations are collected in Table 3. For **1**, the

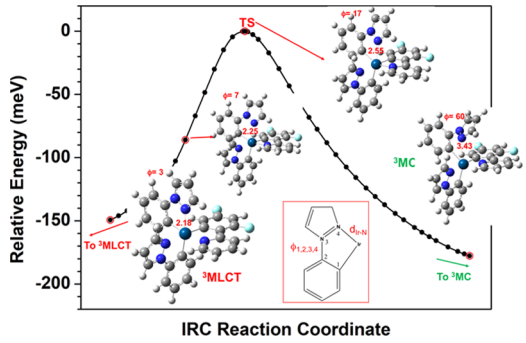

Figure 3. Computed IRC for the ^{3}MLCT → TS → ^{3}MC pathway of **1** (B3LYP/6-31G(d,p)/LANL2DZ). C, N, H, and F atoms in gray, dark blue, white, and light blue, respectively.

Table 3. PWPB95-D3 Activation Barriers (cm^{-1}) for the Rate-Limiting Step of the Temperature-dependent Nonradiative Channels and *A*, Exponential Prefactor (s^{-1}) for 1−3

complex	E_a (cm^{-1})	A (s^{-1})
1	2836[a]	1.47×10^{13}
2	3676	1.70×10^{13}
3	5182	1.97×10^{13}

[a]The rate-limiting step for **1** corresponds to the TS connecting ^{3}MC → ^{3}MC′. For **1**, a more complex thermally activated deactivation channel is found involving ^{3}MLCT, ^{3}MC, ^{3}MC′, and MECP.

computed activation barrier of the limiting step (^{3}MLCT → ^{3}MC) is 2836 cm^{-1}. Experimentally, a Boltzmann analysis of the temperature-dependent photoluminescent decay data was performed and the activation barrier was determined to be 3300 cm^{-1}.[10] To illustrate the problem in the accuracy needed for the rate calculations, the activation barrier was determined to be ca. 1097 cm^{-1}, with the B3LYP functional[18] clearly underestimating the PWPB95-D3 value and the experimental evidences. The exponential prefactor A obtained with the CVT simulations is 1.47×10^{13} s^{-1}. The E_{b-c} values as well as the Boltzmann A_0 prefactors at relevant temperatures are listed in Table S1. The $k_{nr}(T)$ values computed at different temperatures with eq 6 are collected in Table 2. Coming back to the temperature-dependent photoluminescence decay of **1**, the slight lifetime decrease in the 100−200 K regime can be understood as resulting from (i) the increasing thermal population of the triplet substate with the largest k_r value among the three substates of ^{3}MLCT (see the three-spin sublevel contributions in Table S2) and (ii) the slight increase of k_{ISC} with increasing temperatures. In this temperature regime, the computed photoluminescence efficiency achieves a maximum value at 196 K (i.e., 0.38, see Table 2). Importantly, the $k_{nr}(T)$ decay channel becomes only accessible at temperatures above ca. 230 K (see Table 2 and Figure 1). At RT, it becomes the main nonradiative channel and directly competes with radiative decay. Finally, with increasing temperatures (up to 400 K), $k_{nr}(T)$ evolves into the most prominent deactivation channel (see Table 2), and it is thus responsible for the total quench of the photoluminescence at high temperatures. The relevance of the $k_{nr}(T)$ channel is further illustrated in Figure 1b. Hence, by switching off the contribution of the $k_{nr}(T)$ component to eq 2 (dashed line in Figure 1b), the sigmoidlike temperature dependence is lost. Regarding the efficiencies, our calculations predict photoluminescence efficiencies of 0.38 and 0.05 at low temperatures and RT, respectively, in agreement with the experimentally observed drop in efficiencies.

DOI: 10.1021/acs.jpcc.8b00831
J. Phys. Chem. C 2018, 122, 6340−6347

The theoretical Φ_P value at RT of **1** is underestimated with respect to the experimental one, likely due to the computational inaccuracies on the rate calculations (see exemplarily the discussion above regarding the energetic inaccuracies and their exponential relationship in the $k_{nr}(T)$ calculations).

Green-Emitter Case [*fac*-Ir(ppy)$_3$ (2)]. Complex **2** has been extensively studied from both experimental[10,19] and computational viewpoints.[15,18,21,22,26] Therefore, it is the perfect scenario to benchmark our computational approach and to assess its temperature-dependent photoluminescent properties, which have rarely been the target of computational investigations. In Table S3 are collected the computed k_r, k_{ISC}, and $k_{nr}(T)$ decay rates at different temperatures for **2**, whereas the computed plot of the global decay lifetime versus temperature can be found in Figure 4. In this plot, two inflexion points are observable at ca.

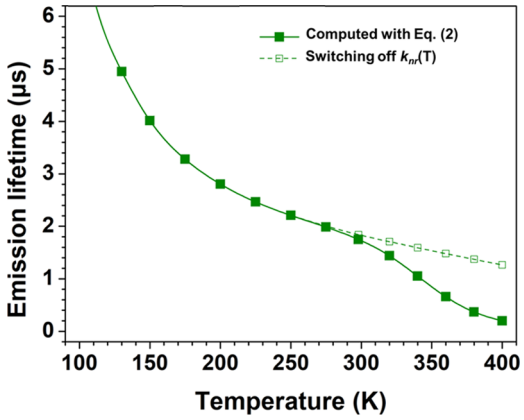

Figure 4. Computed temperature dependence of the photoluminescence decay using eq 2 (bold line) and switching off the $k_{nr}(T)$ component (dashed line) for **2**.

280 and 370 K. In the first temperature regime (100−280 K), there is only direct competition between the k_r and k_{ISC} components because the computed $k_{nr}(T)$ values are negligible (see Table S3). The k_r values are of the same order than those reported in previous works.[15,22] The k_{ISC} decay is mainly promoted by C═C stretching vibration modes and in-plane bending deformations, which are predominantly localized on a single ppy ligand[17] (see in Figure S1, the reorganization energies of the most relevant normal modes for **2**). The IRC of its rate-limiting step, i.e., ^{3}MLCT → TS → ^{3}MC, is shown in Figure S2. The main geometrical changes along this path are analogous to those of **1**. The computed E_a value is 3676 cm^{-1} (see Table 3) and the prefactor A determined by the CVT dynamics is 1.7 × 10^{13} s^{-1}. The E_{b-c} values and the Boltzmann A_0 factors at relevant temperatures are listed in Table S1. Note that the computed barrier for **2** is in agreement with the experiments, larger than that of **1**. The $k_{nr}(T)$ component starts to be non-negligible only beyond RT (compare the dashed and bold computed profiles in Figure 4) and therefore, experimentally, **2** is still highly efficient at RT (Φ_P = 0.97). This is also corroborated by our calculations, which yield a value of 0.72 at RT. This value is quite close to the maximum Φ_P value in the low-temperature regime, i.e., 0.80 at 196 K (see Table 1). Thus, the activation barrier to populate the ^{3}MC channel is large enough to prevent its population in the 100−280 K regime. Conversely, the A value is of the same order for complexes **1** and **2**. Thus, the larger E_a value for **2** is the main feature that prevents the population of the $k_{nr}(T)$ decay channel up to ambient temperatures and hence ensures its large Φ_P value. Above 300 K, the radiative efficiency of complex **2** decreases significantly (see Table S3).

Yellow/Orange-Emitter Case [*fac*-Ir(flpy)$_3$ (3)]. Because of their reduced T_1−S_0 energy gap, yellow, orange, and red Ir(III) complexes are, in this increasing order, more prone to $T_1 \rightarrow S_0$ nonradiative decay than green and blue ones. Conversely, this trend is reversed for the $k_{nr}(T)$ component because a more energetically stabilized T_1 state generally leads to a larger E_a value that prevent the population of the ^{3}MC state for the former complexes. The yellow/orange complex **3** was studied in detail from an experimental point of view by Tsuboyama and co-workers.[20] Relevant experimental and computed photoluminescence data of **3** at cryogenic and room temperatures are collected in Table 1. In Table S4, the computed k_r, k_{ISC}, and $k_{nr}(T)$ decay rates at different temperatures are listed, whereas the plot of the computed global decay lifetime versus temperature is found in Figure 5. The IRC of its ^{3}MLCT → TS → ^{3}MC pathway is shown

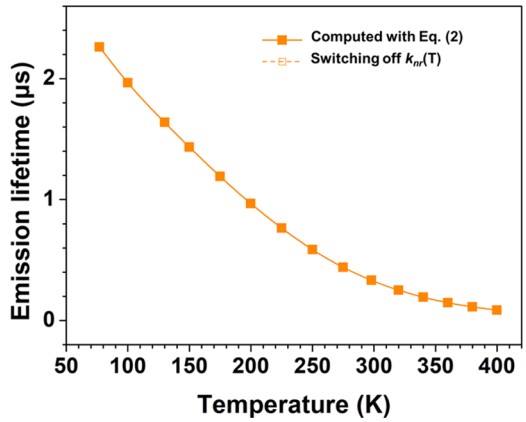

Figure 5. Computed temperature dependence of the photoluminescence decay using eq 2 (bold line) and switching off the $k_{nr}(T)$ component (dashed line) for **3**. Because of the negligible contribution of the $k_{nr}(T)$ component, note that both computed profiles are coincident.

in Figure S4, and it shows identic geometrical distortions to those of **1**−**2**. Finally, the computed E_a and A values are collected in Table 3, whereas the E_{b-c} and A_0 values are reported in Table S1. Complex **3** possesses the largest E_a value among all of the studied complexes (5182 cm^{-1}), thus confirming the initial hypothesis of diminished relevance of the $k_{nr}(T)$ component for yellow-to-red complexes. Indeed, the computed $k_{nr}(T)$ values are negligible in all temperature regimes (77−400 K), see Table S4, and thus the effect of switching off this component has a negligible effect (see in Figure 5). Therefore, the photoluminescence lifetimes of **3** are only determined by a direct competition between the k_r and k_{ISC} components. The computed k_r value (2.5 × 10^5) shows a perfect agreement with its experimental counterpart (see Table 1). The k_{ISC} is promoted by similar aromatic modes to those of **1**−**2** but conversely mainly localized on two ligands (see reorganization energies and the most relevant modes in Figure S3). Note that this complex is characterized by the smallest total reorganization energies amongst all of the complexes. The agreement between the experimental and computed Φ_P value is remarkable (see Table 1). Overall, despite the negligible $k_{nr}(T)$ contribution, smaller Φ_P values are obtained for **3** with respect to **1**−**2**. This trend is observed both computationally and experimentally, and it is due to the confluence of two factors, a smaller k_r value and an enhanced k_{ISC} value for **3**. The smaller k_r value can be rationalized in terms of the more pronounced ligand-centered (^{3}LC)

DOI: 10.1021/acs.jpcc.8b00831
J. Phys. Chem. C 2018, 122, 6340−6347

character of T_1 that leads to smaller SOCs and ZFS values (compare the ΔE splitting between triplet sublevels for all complexes in Table S2). The enhanced ^{3}LC character for **3** is corroborated by the small contribution of the iridium atom to the spin density distribution at the T_1 (see Figure S7). Additionally, despite the small total reorganization energies for **3**, its reduced T_1-S_0 energy gap leads to an enhanced k_{ISC} decay rate as compared to that of **1**−**2**. Therefore, these observations are in accordance to the energy gap law.

METHODS

All of the molecular parameters needed in our model are calculated by density functional theory (DFT). The geometries of the singlet ground state (S_0), the ^{3}MC and ^{3}MLCT triplet excited states, and the transition state (TS) were optimized for complexes **1**−**3** using the hybrid functional B3LYP, in combination with the 6-31G(d,p) atomic basis set for all first and second-row atoms. Relativistic effects were included for the Ir atom using the LANL2DZ pseudopotential. The nature of the stationary points was confirmed by computing the Hessian at the same level of theory. In the case of complex **3**, the two methyl positions of the (9*H*-fluoren-2-yl)pyridine unit were replaced by hydrogen atoms for computational ease. The spin density distributions at the ^{3}MLCT, ^{3}MC, and TS optimized geometries of **1**−**3** are depicted in Figures S5−S7. The $S_0/^3$MC MECP was optimized using Harvey's algorithm, as implemented in the ORCA software,[27] employing the B3LYP functional in combination with the def2-SVP atomic basis set and the ECP-60-mwb Stuttgart/Dresden pseudopotential for Ir. To get accurate energies of E_a, single-point calculations were performed with the dispersion-corrected double-hybrid PWPB95-D3 functional,[28] in combination with the def2-SVP atomic basis and the ECP-60-mwb Stuttgart/Dresden pseudopotential for Ir, as implemented in ORCA. All calculations apart from the MECP optimization and the double-hybrid DFT calculations were carried out with the Gaussian09 program package.[29] The effect of solvation on the geometries and on the computed activation barriers was assessed using tetrahydrofuran (THF) as a solvent and the polarizable continuum model[30] as implemented in Gaussian. These results are presented in Table S5 for **1**. In view of the small differences observed, the gas phase results were used in all of the calculations for all complexes.

To model the $k_{nr}(T)$ decay channel, CVT dynamics was performed. Toward this end, intrinsic reaction coordinate (IRC) calculations of the rate-limiting step, i.e., ^{3}MLCT → TS → ^{3}MC, were carried out at the B3LYP/6-31G(d,p)/LANL2DZ level. Each point along the IRC path was used to build a reliable ^{3}MLCT → TS → ^{3}MC potential energy surface. The CVT dynamics was done with the POLYRATE suite of programs.[31]

The spin−orbit coupling (SOC) was treated as a perturbation, and the exact two-component (X2C) Hamiltonian was applied to construct the SOC operator. For the k_r and k_{ISC} calculations, the SOC calculations were carried out at optimized S_0 geometry with the BDF program package[32] using TD-B3LYP in combination with the 6-31G(d,p) basis set for light atoms and the ANO-RCC-VDZP basis set for iridium atom.

The radiative decay rates of spin sublevels ($k_{r,i}$) are evaluated using Einstein spontaneous emission formula

$$k_{r,i} = \frac{f_i E_{vert,i}^{\ 2}}{1.499\ \mathrm{s\cdot cm^2}} \tag{8}$$

where subscript i denotes the spin sublevel along with its oscillator strength (f_i) and vertical transition energy ($E_{vert,i}$), which are computed at the level of theory stated above using the BDF program package. Boltzmann statistics of these three-spin sublevels is then applied to calculate the overall radiative decay rate (k_r) at different temperatures.

$$k_r = \frac{k_{r,I} + k_{r,II}\exp(-E_{II,I}/k_BT) + k_{r,III}\exp(-E_{III,I}/k_BT)}{1 + \exp(-E_{II,I}/k_BT) + \exp(-E_{III,I}/k_BT)} \tag{9}$$

where $E_{II,I} = E_{vert,II} - E_{vert,I}$ and $E_{III,I} = E_{vert,III} - E_{vert,I}$ are the energy differences between spin sublevels. This thermal rearrangement between the triplet sublevels of ^{3}MLCT originates the temperature dependency of the k_r values at cryogenic temperatures.

For Ir(III) complexes, which are characterized by large SOCs, first-order perturbation theory is a good approximation to compute the nonradiative (k_{ISC}) rate. The k_{ISC} is evaluated using the TVCF theory. Perturbation theory was also applied to compute the nonadiabatic electronic coupling and the spin−orbit couplings. The TVCF formalism makes use of a multidimensional harmonic oscillator model coupled with DFT and TD-DFT calculations, where distortions, displacements, and Duschinsky rotations are taken into account. Thus, the difference between two electronic state potential energy surfaces was considered using $\underline{Q}_e = S\underline{Q}_g + \underline{D}_e$, where S is the Duschinsky rotation matrix; $\underline{Q}_e$ and $\underline{Q}_g$ are the normal-mode coordinates vectors of the S_0 and T_1 states, respectively; and $\underline{D}_e$ is the displacement vector between the minima of the excited and ground-state geometries. Further details can be found in ref 17. The three key parameters governing the k_{ISC} values are: (i) the adiabatic energy gap, (ii) the total reorganization energy, and (iii) the size of SOCs. The k_{ISC} rate calculations were performed with the MOMAP suite of programs.[16,33−37]

CONCLUSIONS

The calculation of the temperature-dependent photoluminescent properties of phosphors has remained elusive up to date. In this manuscript, we report for the first time a general approach to compute the temperature-dependent photoluminescence lifetimes and efficiencies of Ir(III) complexes. Because all possible kinetic scenarios are included within our approach, its validity is not restrained for a limited series of complexes (like previous schemes) but it remains valid for a wide chemical space, i.e., from deep-blue to yellow-to-red phosphors. Importantly, the photoluminescence lifetimes and efficiencies can be estimated at any given temperature and the temperature-dependent photoluminescence decay profiles can be derived. Our future work should be devoted to further improve the estimations of efficiencies in a quantitative basis, which remains difficult due to the computational inaccuracies on the energetics and their exponential relationships in the rate calculations.

Herein, we demonstrate that the strongly temperature-dependent $k_{nr}(T)$ channel is non-negligible up to green complexes. Accordingly, this channel is increasingly less relevant for yellow, orange, and red complexes. In the case of blue complexes, controlling the $k_{nr}(T)$ channel is mandatory to attain large photoluminescence efficiencies at RT. This can be accomplished via stronger Ir−heteroatom bonds that lead to larger E_a values, such as in N-heterocyclic carbene-based Ir(III) complexes. For future blue-phosphor materials design and in view of the computed evidences, an E_a of ca. 4000 cm^{-1} might be

DOI: 10.1021/acs.jpcc.8b00831
J. Phys. Chem. C 2018, 122, 6340−6347

enough to impede the population of the $k_{nr}(T)$ channel at RT. Additionally, this strategy is also beneficial to attain photostable blue Ir(III) emitters.[38] Because of the enormous industrial efforts in obtaining highly efficient phosphors and the increased use of high-throughput approaches on computational materials' design, we anticipate that this protocol will be of great importance for the automatic in silico prescreening of promising PhOLEDs materials.

■ ASSOCIATED CONTENT

Supporting Information

The Supporting Information is available free of charge on the ACS Publications website at DOI: 10.1021/acs.jpcc.8b00831.

Calculated reorganization energies; computed IRC; calculated spin density surfaces of the triplet states (Figures S1−S7), Tables S1−S22 including the *xyz* coordinates of all complexes (PDF)

■ AUTHOR INFORMATION

Corresponding Authors

*E-mail: qpeng@iccas.ac.cn (Q.P.).
*E-mail: zgshuai@tsinghua.edu.cn (Z.S.).
*E-mail: Daniel.Escudero@univ-nantes.fr (D.E.).

ORCID

Denis Jacquemin: 0000-0002-4217-0708
Qian Peng: 0000-0001-8975-8413
Zhigang Shuai: 0000-0003-3867-2331
Daniel Escudero: 0000-0002-1777-8578

Notes

The authors declare no competing financial interest.

■ ACKNOWLEDGMENTS

D.E. thanks funding from the European Union's Horizon 2020 research and innovation programme under the Marie Sklodowska-Curie grant agreement No. 700961. D.J. acknowledges the European Research Council (Marches grant no. 278845) and the RFI Lumomat for financial support. The GRDI-RCTF network is acknowledged for funding short mission travel grants. The work in Beijing is supported by the Ministry of Science and Technology of China through Grant No. 2017YFA0204501 and the National Natural Science Foundation of China through Grant No. 91622121.

■ REFERENCES

(1) Shoichet, B. K. Virtual screening of chemical libraries. *Nature* **2004**, *432*, 862−865.
(2) Curtarolo, S.; Hart, G. L. W.; Nardelli, M. B.; Mingo, N.; Sanvito, S.; Levy, O. The high-throughput highway to computational materials design. *Nat. Mater.* **2013**, *12*, 191−201.
(3) Gómez-Bombarelli, R.; Aguilera-Iparraguirre, J.; Hirzel, T. D.; Duvenaud, D.; Maclaurin, D.; Blood-Forsythe, M. A.; Chae, H. S.; Einzinger, M.; Ha, D.-G.; Wu, T.; et al. Design of efficient molecular organic light-emitting diodes by a high-throughput virtual screening and experimental approach. *Nat. Mater.* **2016**, *15*, 1120−1127.
(4) Shu, Y.; Levine, B. G. Simulated evolution of fluorophores for light emitting diodes. *J. Chem. Phys.* **2015**, *142*, No. 104104.
(5) Adachi, C.; Baldo, M. A.; Thompson, M. E.; Forrest, S. R. Nearly 100% internal phosphorescence efficiency in an organic light-emitting device. *J. Appl. Phys.* **2001**, *90*, 5048−5051.
(6) Jurow, M. J.; Mayr, C.; Schmidt, T. D.; Lampe, T.; Djurovich, P. I.; Brütting, W.; Thompson, M. E. Understanding and predicting the orientation of heteroleptic phosphors in organic light-emitting materials. *Nat. Mater.* **2016**, *15*, 85−91.
(7) Kim, S.-Y.; Jeong, W.-I.; Mayr, C.; Park, Y.-S.; Kim, K.-H.; Lee, J.-H.; Moon, C.-K.; Brütting, W.; Kim, J.-J. Organic Light-Emitting Diodes with 30% External Quantum Efficiency Based on a Horizontally Oriented Emitter. *Adv. Funct. Mater.* **2013**, *23*, 3896−3900.
(8) Kim, K.-H.; Lee, S.; Moon, C.-K.; Kim, S.-Y.; Park, Y.-S.; Lee, J.-H.; Lee, J. W.; Huh, J.; You, Y.; Kim, J.-J. Phosphorescent dye-based supramolecules for high-efficiency organic light-emitting diodes. *Nat. Commun.* **2014**, *5*, No. 4679.
(9) Escudero, D.; Jacquemin, D. Computational insights into the photodeactivation dynamics of phosphors for OLEDs: a perspective. *Dalton Trans.* **2015**, *44*, 8346−8355.
(10) Sajoto, T.; Djurovich, P. I.; Tamayo, A. B.; Oxgaard, J.; Goddard, W. A., III; Thompson, M. E. Temperature Dependence of Blue Phosphorescent Cyclometalated Ir(III) Complexes. *J. Am. Chem. Soc.* **2009**, *131*, 9813−9822.
(11) Yersin, H.; Rausch, A. F.; Czerwieniec, R.; Hofbeck, T.; Fischer, T. The triplet state of organo-transition metal compounds. Triplet harvesting and singlet harvesting for efficient OLEDs. *Coord. Chem. Rev.* **2011**, *255*, 2622−2652.
(12) Deaton, J. C.; Castellano, F. N. Archetypal Iridium(III) Compounds for Optoelectronic and Photonic Applications. In *Iridium(III) in Optoelectronic and Photonics Applications*; Zysman-Colman, Ed.; John Wiley & Sons Ltd: West Sussex, U.K., 2017; pp 1−69.
(13) Baryshnikov, G.; Minaev, B.; Ågren, H. Theory and Calculation of the Phosphorescence Phenomenon. *Chem. Rev.* **2017**, *117*, 6500−6537.
(14) Powell, B. J. Theories of phosphorescence in organo-transition metal complexes − From relativistic effects to simple models and design principles for organic light-emitting diodes. *Coord. Chem. Rev.* **2015**, *295*, 46−79.
(15) Kleinschmidt, M.; van Wüllen, C.; Marian, M. Intersystem-crossing and phosphorescence rates in *fac*-$Ir^{III}(ppy)^3$: A theoretical study involving multi-reference configuration interaction wavefunctions. *J. Chem. Phys.* **2015**, *142*, No. 094301.
(16) Shuai, Z.; Peng, Q. Excited states structure and processes: Understanding organic light-emitting diodes at the molecular level. *Phys. Rep.* **2014**, *537*, 123−156.
(17) Peng, Q.; Niu, Y.; Shi, Q.; Gao, X.; Shuai, Z. Correlation Function Formalism for Triplet Excited State Decay: Combined Spin−Orbit and Nonadiabatic Couplings. *J. Chem. Theory Comput.* **2013**, *9*, 1132−1143.
(18) Escudero, D. Quantitative prediction of photoluminescence quantum yields of phosphors from first principles. *Chem. Sci.* **2016**, *7*, 1262−1267.
(19) Hofbeck, T.; Yersin, H. The Triplet State of *fac*-$Ir(ppy)_3$. *Inorg. Chem.* **2010**, *49*, 9290−9299.
(20) Tsuboyama, A.; Iwawaki, H.; Furugori, M.; Makaide, T.; Kamatani, J.; Igawa, S.; Moriyama, T.; Miura, S.; Takiguchi, T.; Okada, S.; et al. Homoleptic Cyclometalated Iridium Complexes with Highly Efficient Red Phosphorescence and Application to Organic Light-Emitting Diode. *J. Am. Chem. Soc.* **2003**, *125*, 12971−12979.
(21) Mori, K.; Goumans, T. P. M.; van Lenthe, E.; Wang, F. Predicting phosphorescent lifetimes and zero-field splitting of organometallic complexes with time-dependent density functional theory including spin−orbit coupling. *Phys. Chem. Chem. Phys.* **2014**, *16*, 14523.
(22) Younker, J. M.; Dobbs, K. D. Correlating Experimental Photophysical Properties of Iridium(III) Complexes to Spin−Orbit Coupled TDDFT Predictions. *J. Phys. Chem. C* **2013**, *117*, 25714−25723.
(23) Peng, Q.; Shi, Q.; Niu, Y.; Yi, Y.; Sun, S.; Li, W.; Shuai, Z. Understanding the efficiency drooping of the deep blue organometallic phosphors: a computational study of radiative and non-radiative decay rates for triplets. *J. Mater. Chem. C* **2016**, *4*, 6829−6838.
(24) Fernández-Ramos, A.; Miller, J. A.; Klippenstein, S. J.; Truhlar, D. G. Modeling the Kinetics of Bimolecular Reactions. *Chem. Rev.* **2006**, *106*, 4518−4584.
(25) Steinmetz, M.; Grimme, S. Benchmark Study of the Performance of Density Functional Theory for Bond Activations with (Ni,Pd)-Based Transition-Metal Catalysts. *ChemistryOpen* **2013**, *2*, 115−124.

DOI: 10.1021/acs.jpcc.8b00831
J. Phys. Chem. C 2018, 122, 6340−6347

(26) Jansson, E.; Minaev, B.; Schrader, S.; Ågren, H. Time-dependent density functional calculations of phosphorescence parameters for *fac*-tris(2-phenylpyridine) iridium. *Chem. Phys.* **2007**, *333*, 157−167.
(27) Neese, F. *Orca, an Ab Initio, DFT and Semiempirical SCF-MO Package 2.8.0 R2327*; University of Bonn: Bonn, Germany, 2011.
(28) Goerigk, L.; Grimme, S. Efficient and Accurate Double-Hybrid-Meta-GGA Density Functionals—Evaluation with the Extended GMTKN30 Database for General Main Group Thermochemistry, Kinetics, and Noncovalent Interactions. *J. Chem. Theory Comput.* **2011**, *7*, 291−309.
(29) Frisch, M. J.; Trucks, G. W.; Schlegel, H. B.; Scuseria, G. E.; Robb, M. A.; Cheeseman, J. R.; Scalmani, G.; Barone, V.; Menucci, B.; Petersson, G. A. et al. *Gaussian 09*, revision A.1; Gaussian, Inc.: Wallingford, CT, 2009.
(30) Tomasi, J.; Mennucci, B.; Cammi, R. Quantum Mechanical Continuum Solvation Models. *Chem. Rev.* **2005**, *105*, 2999−3094.
(31) Zheng, J. et al. *POLYRATE*, version 2010; University of Minnesota: Minneapolis, MN, 2010.
(32) Liu, W.; Wang, F.; Lemin, L. The Beijing Density Functional (BDF) Program Package: Methodologies and Applications. *J. Theor. Comput. Chem.* **2003**, *02*, 257−272.
(33) Shuai, Z.; Peng, Q.; Niu, Y. L.; Geng, H. *MOMAP, a Free and Open-Source Molecular Materials Property Prediction Package*, revision 0.2.004; Shuai group: Beijing, CN, 2014, http://www.shuaigroup.net/.
(34) Peng, Q.; Yi, Y.; Shuai, Z.; Shao, J. Excited state radiationless decay process with Duschinsky rotation effect: Formalism and implementation. *J. Chem. Phys.* **2007**, *126*, No. 114302.
(35) Peng, Q.; Yi, Y.; Shuai, Z.; Shao, J. Toward quantitative prediction of molecular fluorescence quantum efficiency: Role of Duschinsky rotation. *J. Am. Chem. Soc.* **2007**, *129*, 9333−9339.
(36) Niu, Y.; Peng, Q.; Shuai, Z. Promoting-mode free formalism for excited state radiationless decay process with Duschinsky rotation effect. *Sci. China, Ser. B: Chem.* **2008**, *51*, 1153−1158.
(37) Niu, Y.; Peng, Q.; Deng, C.; Gao, X.; Shuai, Z. Theory of Excited State Decays and Optical Spectra: Application to Polyatomic Molecules. *J. Phys. Chem. A* **2010**, *114*, 7817−7831.
(38) Jacquemin, D.; Escudero, D. The short device lifetimes of blue PhOLEDs: insights into the photostability of blue Ir(III) complexes. *Chem. Sci.* **2017**, *8*, 7844−7850.

DOI: 10.1021/acs.jpcc.8b00831
J. Phys. Chem. C 2018, 122, 6340−6347